

# Enhanced Gas Recovery by CO<sub>2</sub> injection: Influence of monovalent and divalent brines and their concentrations on CO<sub>2</sub> dispersion in porous media

Muhammad Kabir Abba

Spray Research Group (SRG), School of Science, Engineering and Environment (SEE),  
University of Salford, Manchester, M5 4WT, UK

## Abstract

This study aims to experimentally investigate the roles of different brine types and concentrations on the longitudinal dispersion coefficient ( $K_L$ ) during enhanced gas recovery by CO<sub>2</sub> injection. Core flooding process was used to simulate the displacement of CH<sub>4</sub> by supercritical CO<sub>2</sub> in a *Buff Berea* core sample at a pressure and temperature of 1400 psig and 50°C respectively, and a CO<sub>2</sub> injection rate of 0.3 ml/min. Individual NaCl, KCl, CaCl<sub>2</sub> and MgCl<sub>2</sub> solutions were prepared as test brines with ionic strengths (IS) of 1M, 2M, and 3M. The results revealed that, at lower IS of 1M, MgCl<sub>2</sub> and CaCl<sub>2</sub> brines had the lowest  $K_L$  while the monovalent brines showed relatively higher  $K_L$ . Divalent brines showed a higher degree of salting out effects at higher concentrations resulting in higher  $K_L$ . The salting and drying out effects of divalent brines were responsible for higher CH<sub>4</sub> recovery at 2M IS as CH<sub>4</sub> comes out of solution. A hyperbolic-type relationship exists between the two properties ( $K_L$  and IS), where  $K_L$  decreases from 0 to 1M IS, and then increases sharply at IS >1M – this behaviour is most pronounced in the divalent brines. Lowest contamination of the recovered CH<sub>4</sub> was found to be between formation water salinities of 5-15 wt.%, regardless of salt type, during EGR by CO<sub>2</sub> injection and sequestration. This study will not only present new knowledge on EGR process but will also provide an avenue for establishing a screening criterion based on formation water salinity for effective EGR process. This is a first experimental investigation which establishes the relationship between salt types and concentration and the  $K_L$  in porous media.

**Keywords:** Enhanced gas recovery; ionic strength; Connate water salinity; dispersion coefficient; CO<sub>2</sub> sequestration

## 1 Introduction

Anthropogenic greenhouse gas (GHG) emissions are the main causes of global warming as a consequence of climate change. Carbon dioxide (CO<sub>2</sub>) as a GHG accounts for up to 64% of the accrued negative effects on the environment (Ding et al., 2018), given that it is the most abundant anthropogenic GHG emission in the world (U.S. EPA, 2019). Several abatement strategies are proposed to reduce the carbon emission footprint from various industries. These approaches include the shifting of energy mix to alternative less carbon intensive sources, energy efficiency, and carbon capture and underground storage (CCUS) (Kumar et al., 2020). The former two approaches are not enough to mitigate the carbon footprint given that organic sources of energy (petroleum) will still be relevant and the wholly shift away from them in the near future is almost impossible. Therefore, a pragmatic approach that is gaining attention globally is carbon capture and underground storage (Raza et al., 2017). This involves capturing

the CO<sub>2</sub> and safely sequestering it in underground structures. These underground structures include (i) coal bed methane, (ii) un-mineable coal seams, (iii) shale formations, (iv) deep saline aquifers (v) depleted oil and gas reservoirs (Bennaceur, 2013; Benson and Cole, 2008; Feather and Archer, 2010; Kalantari-Dahaghi et al., 2013; Oldenburg, 2003; Oldenburg and Benson, 2002; Zhang and Song, 2013a, 2013b). Depleted oil and gas reservoirs have the potential to provide substantial storage sites and additional economic incentives through enhanced oil/gas recovery technology (Ding et al., 2018; Kalra and Wu, 2014). Conventional natural gas reservoirs, thus, have more advantages in the form of reservoir integrity (Kalra and Wu, 2014), as natural gas reservoirs have contained natural gas for long periods and their extraction does not require complex processes to recover the natural resource unlike oil reservoirs through enhanced oil recovery techniques. This is one of the reasons why natural gas reservoirs present the ideal sequestration sites for CO<sub>2</sub>. Substantial volumes of CO<sub>2</sub> can be sequestered, and additional natural gas can be obtained which will augment part of the cost of the sequestration process.

The EGR technology, however, is not without its drawbacks, mostly in the form of the contamination of recovered natural gas (CH<sub>4</sub>) by the injected CO<sub>2</sub> from the depleted natural gas reservoir, which is the selling point of the technology. The offset of the cost of the sequestration process from the recovered gas will be at risk, as the injected CO<sub>2</sub> may contaminate the natural gas recovered as a result of mixing. This is due to the gas-gas displacement process of EGR where the gases (CO<sub>2</sub> and CH<sub>4</sub>) are thermodynamically similar (Honari et al., 2013). Thus, there is no distinct property gradient that will be taken advantage of, to effect displacement without mixing. Several factors are responsible for the excessive mixing between the injected CO<sub>2</sub> and nascent CH<sub>4</sub>. Core-scale laboratory investigations are available in literature which evaluated the phenomenon of mixing in consolidated porous media and sand packs caused by different factors. Some of the investigated factors/parameters include the effects of injected CO<sub>2</sub> purity on the displacement process during EGR (Nogueira and Mamora, 2005; A. T. Turta et al., 2007), reservoir heterogeneity (Honari et al., 2015; S Sim et al., 2009), injection orientation and petrophysical properties variation (Abba et al., 2018a; Abba et al., 2019b; Liu et al., 2015, 2018; Sim Sim et al., 2009; Zhang et al., 2014), injection rates (Hughes et al., 2012), temperature and pressure (Liu et al., 2020), relative permeability and sweep efficiency (Al-Abri et al., 2012), connate water presence and salinity (Abba et al., 2018b; Honari et al., 2016). Understanding these parameters as they relate to the insitu mixing between the gases and their interaction with the porous media is vital to a successful implementation and adoption of any CO<sub>2</sub>-EGR process. One of the scenarios that have not been investigated widely is the presence of connate water. It has been established that this property has significant influence on the dispersion coefficient of CO<sub>2</sub> injectivity (Abba et al., 2018b; Honari et al., 2016) and storability of the CO<sub>2</sub> for EGR process (Abba et al., 2019a). The nature of the connate water is also fundamental, in that, different species of salts exist in the connate water brine and have different properties and effects on the interacting fluids at reservoir conditions.

A summary of previous works which considered the presence of connate water during fluid dispersion in a CO<sub>2</sub>–CH<sub>4</sub> system only in porous media is shown in Table 1. Turta et al. (2007) realised higher methane recovery which they attributed to the presence of connate water

saturation leading to CO<sub>2</sub> dissolution and also the narrowing of the pore spaces - enhancing the homogeneity of flow of the fluids within the pore matrix. Sidiq et al. (2009) investigated dispersion of a blend of CH<sub>4</sub> and CO<sub>2</sub> into a CH<sub>4</sub> – CO<sub>2</sub> mixture in the presence of 25,000 mg/L brine at 12.4% brine saturation in a sandstone core sample. However, they did not evaluate dispersion as a function of the presence of connate water and there was no data for dispersion in dry cores to make comparison. Honari et al. (2016) were the first to establish the relationship between fluid dispersion and irreducible water saturation in a CH<sub>4</sub> – CO<sub>2</sub> system in carbonate and sandstone rock cores. They observed that there was substantial increase in dispersion in both types of core samples in the presence of deionised water as the simulated formation fluid. Irreducible water occupied smaller pore spaces along the core axis as confirmed by NMR measurements. This in turn created narrower pore spaces and more tortuous flow paths thereby increasing the dispersion of the fluids. Similar trend was observed in the works of Abba et al. (2017) where they reported an increase in dispersion in a CH<sub>4</sub> – CO<sub>2</sub> system when a NaCl brine with 20 wt% concentration was used as the formation brine. This further narrowed and eventually plugged off the smaller pore spaces of the sandstone core sample used; indicated by the increase in differential pressures during flooding compared to the experiment with distilled water. Abba et al. (2018b) further investigated dispersion in distilled water and NaCl brine with salinity of 15 wt% in a CH<sub>4</sub> – CO<sub>2</sub> system. They reported that CO<sub>2</sub> dispersion in CH<sub>4</sub> decreased as connate water salinity increased from 0 to 15 wt% NaCl. An interplay between the connate water salinity and saturation and their variation was investigated by Abba (2018). His findings recounted that decrease in dispersion was observed between CO<sub>2</sub> and CH<sub>4</sub> as salinity increased from 5 – 10wt% and was similar at different NaCl brine saturations.

*Table 1 Summary of existing experimental works on brine types, salinity, presence, and concentration on fluid dispersion of CO<sub>2</sub>-CH<sub>4</sub> system in porous media*

<b>System</b>	<b>Brine type and concentration</b>	<b>Inference</b>	<b>Saturation</b>	<b>Reference</b>
<b>CH<sub>4</sub> – CO<sub>2</sub>, N<sub>2</sub> – CO<sub>2</sub></b>	Not specified	Higher CH <sub>4</sub> recovery in both systems. Increase in dispersion.	17 – 25 %	(Turta et al., 2007)
<b>CH<sub>4</sub> – CO<sub>2</sub></b>	NaCl, 25,000 mg/L	No direct relation of Sw to dispersion reported.	12.4 %	(Sidiq and Amin, 2009)
<b>CH<sub>4</sub> – CO<sub>2</sub></b>	Deionised H <sub>2</sub> O	Significant increase in dispersion due to irreducible water saturation.	41 – 62 %	(Honari et al., 2016)
<b>CH<sub>4</sub> – CO<sub>2</sub></b>	Deionised H <sub>2</sub> O	Dispersivity increases with water content.	10 – 43 %	(Zecca et al., 2017)
<b>CH<sub>4</sub> – CO<sub>2</sub></b>	Distilled H <sub>2</sub> O, NaCl, 0 and 20 wt. %	Higher dispersion observed at higher concentration.	10 %	(Abba et al., 2017)
<b>CH<sub>4</sub> – CO<sub>2</sub></b>	Distilled H <sub>2</sub> O, NaCl, 0, 5, 10 wt. %	Dispersion decreased from 0 wt% to 10wt%.	10 %	(Abba et al., 2018b)

<b>CH<sub>4</sub> – CO<sub>2</sub></b>	Distilled H <sub>2</sub> O, NaCl, 0, 5, 10 wt. %	Dispersion was higher at higher water saturation but decreased with increase concentration.	5 – 10 %	(Abba, 2018)
--	--	---	----------	--------------

CO<sub>2</sub> and CH<sub>4</sub> exhibit distinctive characteristics in terms of solubility in different brine types, concentrations and composition. This will influence the flow behaviour of the interacting fluids in the porous medium during EGR when considering a dynamic ternary system. Formation brine consists of different salt species with different ion types; divalent and monovalent. Divalent brines have been found to exhibit a strong salting out effect in the presence of CO<sub>2</sub> compared monovalent brines (Tong et al., 2013). This phenomenon will most assuredly have substantial effects on the intricacies and channels of the pore matrix in a porous medium. Consequently, reservoir properties like permeability and porosity will be affected and their reduction/impairment will be very eminent. This restriction to flow will eventually increase the interstitial velocity of the CO<sub>2</sub> as it traverses the core sample, thereby increasing the chances of higher rates of mixing between the injected CO<sub>2</sub> and insitu CH<sub>4</sub>. Furthermore, solubility of divalent salts (MgCl<sub>2</sub> and CaCl<sub>2</sub>) of the same molality were reported to be similar at different conditions of temperature and pressure as shown in the works of Tong et al (2013). They concluded that ion charge was overwhelmingly more important in terms of salting out effects than ion size (monovalent salts have larger ion size). Thus, the justification for the adoption of ionic strength, in this study, as opposed to molarity of the brines. Importantly, this phenomenon will play a significant role in EGR as changes will occur in the pore matrix during the displacement process. The individual impact of monovalent and divalent salt types and concentrations on the dispersion is, however, limited. Thus, this study will highlight the relationship between the type of salt species and the dispersion coefficient of CO<sub>2</sub> during EGR in conventional consolidated sandstone porous media.

To the author's knowledge, this is the first ever research of its kind which capitalises on the effect on salt types and concentration on CO<sub>2</sub> dispersion in a CO<sub>2</sub> – CH<sub>4</sub> system in consolidated porous media. The study will provide additional knowledge to enable successful implementation of CO<sub>2</sub> sequestration during EGR for the purpose of decarbonisation and also postulate a screening criterion for CO<sub>2</sub> storage in natural gas reservoirs. This will not only reduce the carbon emissions from the oil and gas industry but will also alleviate and dispel the fears and sentiments towards the oil and gas industry with regards to pollution when EGR technology becomes widely accepted.

## 1.1 Dispersion Theory

Dispersion is defined as the irreversible mixing of two miscible fluids during a displacement process (Adepoju et al., 2013). Two simultaneous displacement mechanisms are responsible for dispersion – molecular diffusion and mechanical dispersion (Perkins and Johnston, 1963) and occur as a consequence of difference in velocity and concentration gradients. Dispersion coefficient is a measure of the rate of mixing between the two fluids during a displacement process. The main convective flux is the longitudinal dispersion coefficient, denoted by  $K_L$ ,

and has the largest value compared to the transverse dispersion,  $K_T$  which occurs perpendicular to the  $K_L$ .  $K_T$  is often neglected because it is significantly lower than the  $K_L$  and very difficult to obtain experimentally. Therefore, (Newberg and Foh, 1988) came up with a single parameter diffusion-type 1D advection dispersion equation (ADE) used in gas transport in porous media and it is shown in Eq. (1).

$$\frac{\partial C}{\partial t} = K_L \frac{\partial^2 C}{\partial x^2} - u \frac{\partial C}{\partial x} \quad 1$$

Where,  $C$  is the CO<sub>2</sub> concentration at location  $x$  at time  $t$ ,  $K_L$  (m<sup>2</sup>/s) is the coefficient of longitudinal dispersion, and  $u$  is the interstitial velocity (m/s). It is based on the assumption that the dispersion coefficient and interstitial velocity are independent on the concentration of CO<sub>2</sub>,  $C$ .

The dimensionless solution to Eq. (1) maybe shown as follows:

$$C = \frac{1}{2} \left\{ \operatorname{erfc} \left( \frac{x_D - t_D}{2\sqrt{t_D/P_e}} \right) + e^{P_e x_D} \operatorname{erfc} \left( \frac{x_D + t_D}{2\sqrt{t_D/P_e}} \right) \right\} \quad 2$$

Where  $Pe = uL/K_L$ , the Peclet Number defined as the ratio of convection to dispersion,  $L$  is the length of core sample,  $tD = (tu/Le)$  – dimensionless time,  $Le$  is experimental length,  $xD = x/Le$  – dimensionless distance.

The analytical solution to the 1D ADE (Eq. 2) will be fitted to the CO<sub>2</sub> concentrations profiles obtained from core flooding experiments in terms of the *Péclet* number to evaluate the corresponding dispersion coefficient. The evaluated dispersion coefficient is the value which provides the best fit or agreement between the experimental data and the analytical solution.

## 2 Experimental method

### 2.1 Materials used

High purity CH<sub>4</sub> (99.995%) and research grade CO<sub>2</sub> were obtained from BOC UK and used for the study. General purpose grade sodium chloride (NaCl), Potassium chloride (KCl), Magnesium chloride (MgCl<sub>2</sub>) and Calcium chloride (CaCl<sub>2</sub>) salts from Sigma Aldrich UK were used to prepare the brines to simulate reservoir formation water for the experiments. *Buff Berea* sandstone core sample used in this study was obtained from Kocurek Industries USA, and has permeability of 420.2 md, porosity of 0.23, and a length and diameter of 75.22 mm and 24.81 mm respectively.

### 2.2 Apparatus and Procedure

#### 2.2.1 Brine preparation and core sample saturation

Prior to the core flooding process, different brines, with different ionic strengths, were prepared to evaluate the influence of ionic strength on the dispersion of CO<sub>2</sub> during EGR. These are shown in Table 2. The choice of brine preparation according to the ionic strengths was to highlight the prevalence of ionic charge over ion size in prompting salting out effect in the presence of CO<sub>2</sub> as explained in the findings of Tong et al (2013).

*Table 2 Brine types showing different ionic strengths*

<b>Ionic Strength (M)</b>	<b>Salt type</b>	<b>Concentration (g/L)</b>
1	NaCl	58.7
	CaCl <sub>2</sub>	37.0
	MgCl <sub>2</sub>	30.6
	KCl	74.5
2	NaCl	117.0
	CaCl <sub>2</sub>	74.0
	MgCl <sub>2</sub>	61.4
	KCl	149
3	NaCl	175.5
	CaCl <sub>2</sub>	111.0
	MgCl <sub>2</sub>	92.3
	KCl	224.0

Porosity was evaluated using Helium porosimetry. Equipment description and procedure can be found elsewhere (Abba et al., 2018b). External brine saturation, with the desired brine, of the core sample was carried out after cleaning using Soxhlet extraction and oven drying. A vacuum saturation chamber, shown in Figure 1, was used to saturate the core sample externally to ensure full brine saturation of the core sample.

### **2.2.2 Core flooding**

The setup of the core flooding equipment and operating principle and procedure was adopted from our previous works (Abba et al., 2019a; Abba et al., 2018b). The setup is shown in Figure 2 has a combined uncertainty in measurement of 2% and designed and operated based on the API standard. After the external saturation, the core sample was wrapped in aluminium foil to avoid permeation of CO<sub>2</sub> into the *viton* sleeve and into the overburden hydraulic oil, simulating the confining pressure. Before the core sample was wrapped in the aluminium foil, it was wrapped in cling film to prevent the foil from sticking to the core sample. This was noticed in previous experiments where a reaction between the supercritical CO<sub>2</sub> and the foil at the operating conditions occurred which made the foil stick permanently to the core sample preventing reuse of the core sample for subsequent experiments. The experimental conditions of 1400 psig and 50°C were adopted from the work of Liu et al. (2015) and the injection rate of 0.3 ml/min was taken from Abba et al. (2018).

The core sample was then loaded into the hassler-type core holder and flooded with the same brine that was used in the external saturation. A stepwise bump in the injection rate from 0.5ml/min to 2 ml/min was adopted to ensure full saturation, and this was realised when the differential pressure (dP) became constant at each injection rate bump. Then a drainage experiment was performed where CH<sub>4</sub> was injected into the saturated core sample at 0.2 ml/min to establish initial water saturation ( $S_{wi}$ ). After the desired pressure of 1400 psig was attained, and there was no more being produced/collected in the test tube at the downstream of the backpressure regulator, the drainage experiment was stopped. At the onset of the drainage experiment, the temperature was set to 50°C and the connecting tubings were wrapped in an insulation jacket to ensure that as the displacement process begins, the CO<sub>2</sub> will remain in its supercritical state upon entry into the core sample to reduce the entry artefacts. The displaced brine was collected and recorded and was used to evaluate the  $S_{wi}$ . Same procedure was carried out for all the brine types.

The displacement experiment was then initiated at 0.3 ml/min constant injection rate, and gas sampling and analysis were performed on a gas chromatography (GC) set-up where a *method* sequence was designed to sample, at 4 minutes intervals, the core flooding effluents to generate the concentration profiles of the experiments. After there was insignificant/negligible amount of CH<sub>4</sub> in the gas sampling spectrum in the GC, the core flooding process was then stopped, and the system was depressurised. The core sample was then removed and cleaned. Methanol was used in the Soxhlet extraction to remove any residual precipitated salts and the core sample was reused for subsequent tests. Prior to that, the porosity was evaluated to ensure there were no salt deposits. To ensure good repeatability, each test was performed three times before the method was adopted for the actual test.

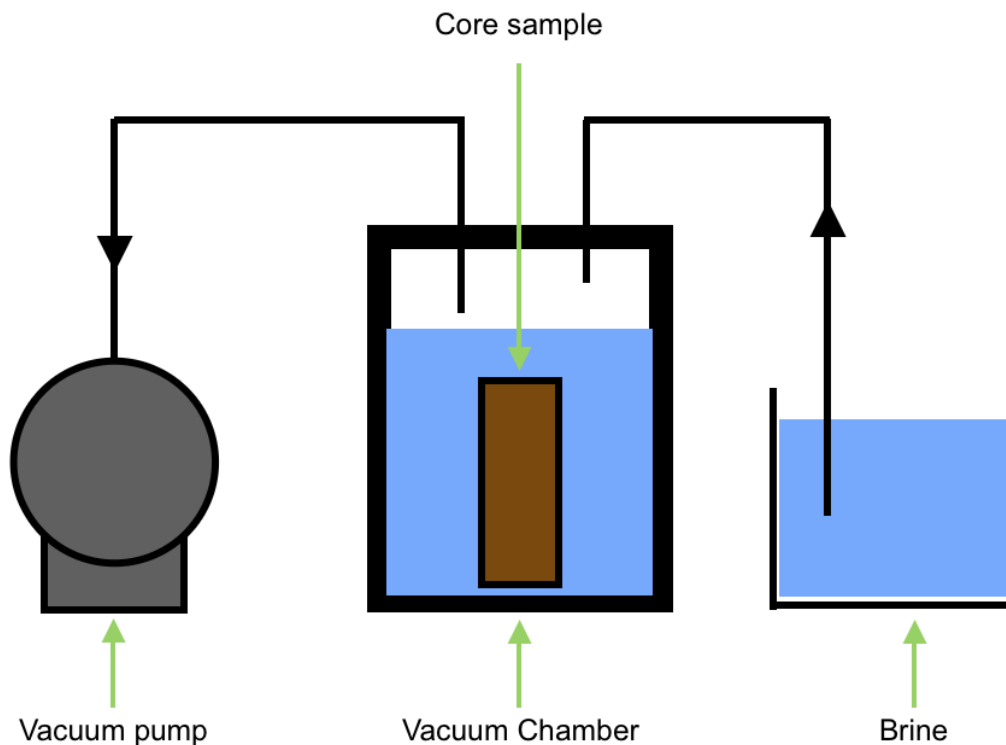


Figure 1 Brine saturation chamber set-up

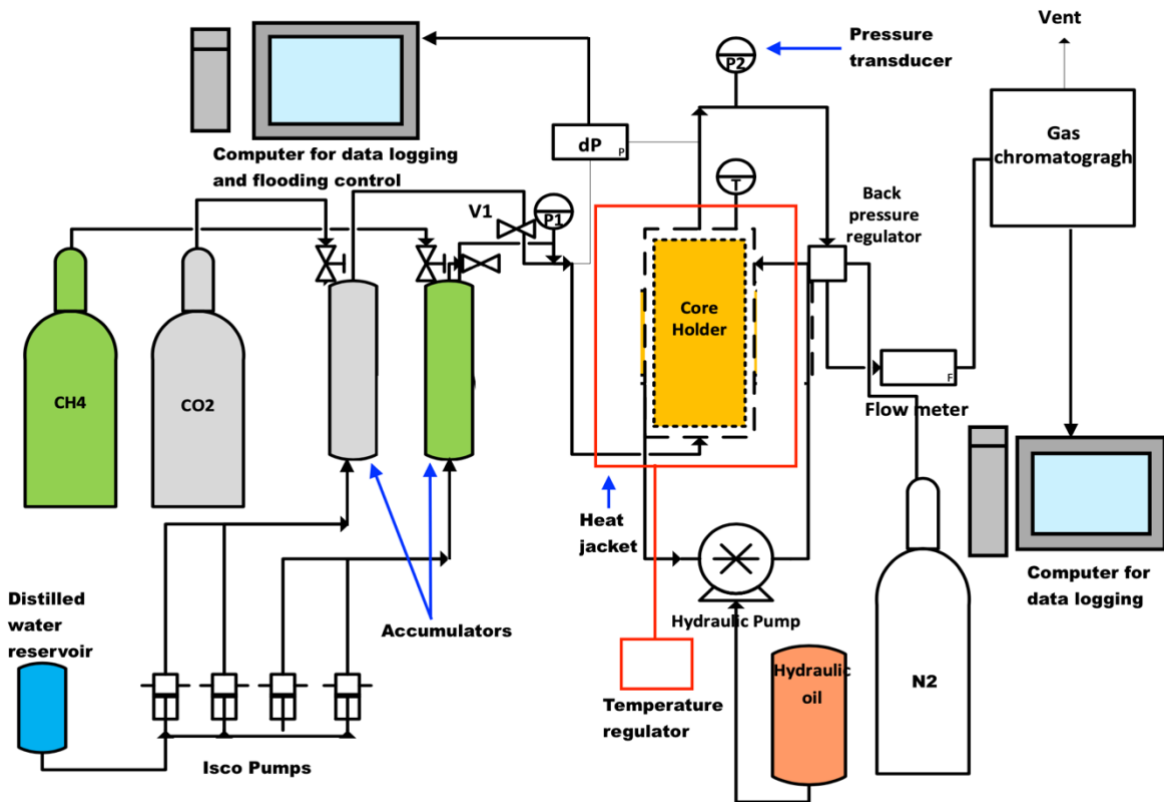


Figure 2 Schematics of core flooding equipment integrated with a gas chromatograph

### 3 Results and discussion

#### *Repeatability and reproducibility of experiment*

Prior to the actual test, three (3) experimental runs were repeated on the same core sample (*Buff Berea*) at the same operating conditions of 1400 psig, 50°C and 0.3 ml/min to evaluate the repeatability of the experiment. The fitted dispersion coefficients for Test 1, Test 2, and Test 3 are  $3.49 \times 10^{-8} \text{ m}^2/\text{s}$ ,  $3.87 \times 10^{-8} \text{ m}^2/\text{s}$ , and  $3.89 \times 10^{-8} \text{ m}^2/\text{s}$  respectively. The standard deviation in the dispersion coefficients is 6.01% with an average relative difference of 4.62%. This shows that the experimental set up and methodology in this study have good reliability and reproducibility. The concentration profile for the repeatability experiments is shown in Figure 3.

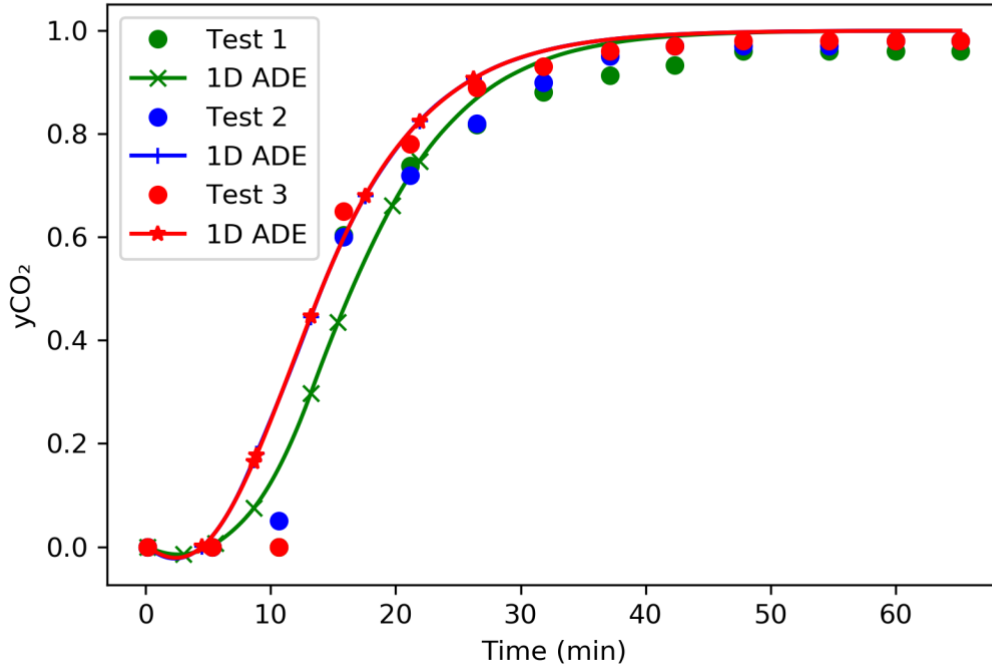


Figure 3 Repeatability and reliability tests concentration profiles

### 3.1 Dispersion coefficient

The concentration profiles for each brine scenario were obtained from the core flooding experiments and the gas analysis from the GC set up. Eq. (2) was used to curve fit the experimental data to evaluate the longitudinal dispersion coefficient,  $K_L$ . The  $K_L$  was used as the fitting parameter in the Least Squares Regression.  $L_e$  in Eq. (2) was also adjusted to obtain better fit of the 1D ADE to the experimental data, given that one of the assumptions in Eq. (2) is that the interstitial velocity,  $u$ , is constant and thus, it was kept constant in the regression. Python was used for the least-squares regression analysis and curve fitting using all the relevant libraries in the *Jupyter* notebook and data visualisation in this experimental work. The code used for the curve fitting in this work is provided in the supplementary file.

Distilled water was used to saturate the core sample and used as the benchmark for the subsequent experiments. This was taken to be the simulated formation water with 0M ionic strength. Figure 4 shows the 1D ADE fitted experimental data for different salts at 1M ionic strength test. As can be seen, late breakthrough of the injected  $\text{CO}_2$  was realised with the distilled water flooding scenario. This can be attributed to (i) the level of saturation of distilled water (see Table 3) in the core sample which provided larger volumes of aqueous solution for the  $\text{CO}_2$  to interact with and (ii) extremely high solubility of supercritical  $\text{CO}_2$  in distilled water (Ahmad et al., 2016; Rochelle and Moore, 2002). So, a reasonable volume of  $\text{CO}_2$  was dissolved in the formation distilled water and substantial storage was achieved. Contrary to the distilled water scenario, the KCl scenario showed an early breakthrough of  $\text{CO}_2$  albeit an appearance of a gentler curve compared to the others, indicating that the displacement front was wider (Ekwere, 2007) and larger and thus, higher mixing. In terms of solubility, it has been

established that CO<sub>2</sub> has higher solubility in monovalent salts than divalent salt (Messabeb et al., 2017). Therefore, a possible explanation of this effect observed is that the concentration of the KCl at that ionic strength is higher than the rest, taking into account the nature of the salt. This is shown in Figure 7. Higher brine concentration translates to higher density. So, the KCl brine will occupy narrow pore spaces within the pore matrix and reduce the tortuosity of the core sample and hence, the CO<sub>2</sub> will create a rather direct path from the inlet of the core sample and exit at the outlet without a substantial interaction with the formation brine. Therefore, the  $K_L$  for the KCl test is highest amongst the other tests at 1M ionic strength. Distilled water followed next with  $2.81 \times 10^{-8} \text{m}^2/\text{s}$  as shown in Table 3. Distilled water, with the absence of any additive salts (lower density), does not entirely plug off the narrow pore channels and as such, only reduces the sizes of the pore throats and make them narrower. This, thus, increases the interstitial velocity of the injected CO<sub>2</sub> as it traverses the core sample and by implication, the  $K_L$  becomes relatively high. CaCl<sub>2</sub> has the lowest  $K_L$  in this flooding scenario, as its density is not as low as that of distilled water and not as high as those of NaCl and KCl. It can be presented that the tortuosity of the core sample during the CaCl<sub>2</sub> displacement process was reduced such that the CO<sub>2</sub> navigated smoothly as it displaced the CH<sub>4</sub> and interacted more amply with the formation brine. Correspondingly, MgCl<sub>2</sub> runs exhibited lower  $K_L$  and the same explanation as the CaCl<sub>2</sub> applies to this scenario.

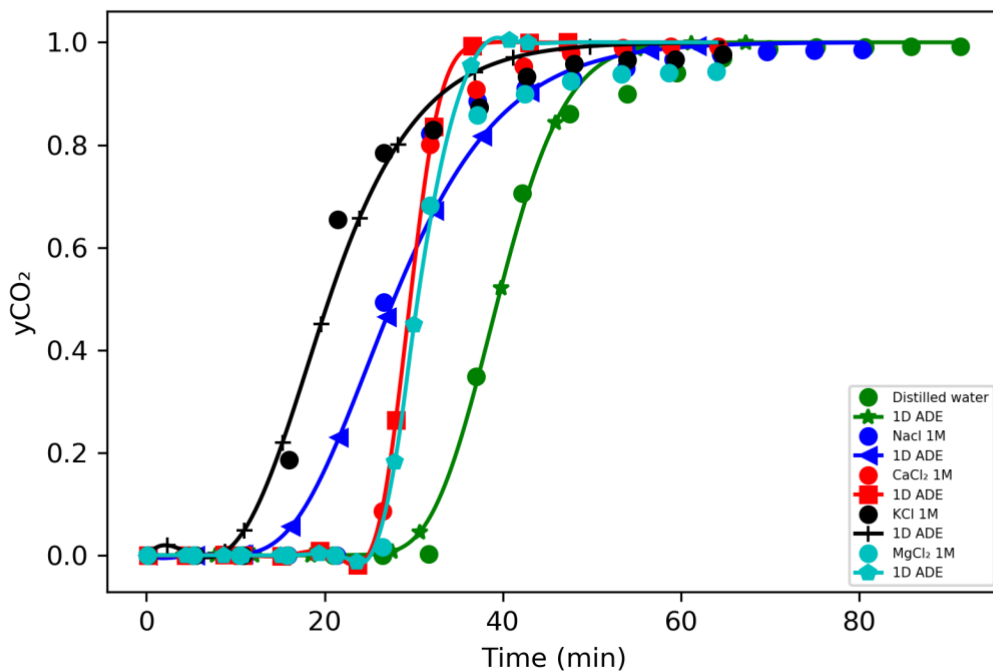


Figure 4 CO<sub>2</sub> Concentration profile at 1M ionic strength for different salt types

Table 3 Dispersion coefficients of all experimental runs

Scenario	Ionic strength (M)	Swi (%)	Pressure (psig)	Temperature (°C)	Interstitial Velocity ( $10^{-5}$ m/s)	$K_L$ ( $10^{-8}$ m <sup>2</sup> /s)
Distilled	0	44.2	1400	50	4.50	2.81
NaCl	1	32.3	1400	50	4.50	2.54
	2	34.1	1400	50	4.50	3.30
	3	34.8	1400	50	4.50	4.09
CaCl <sub>2</sub>	1	33.7	1400	50	4.50	0.69
	2	32.2	1400	50	4.50	3.70
	3	34.7	1400	50	4.50	9.98
KCl	1	31.3	1400	50	4.50	4.13
	2	30.2	1400	50	4.50	6.54
	3	29.4	1400	50	4.50	9.17
MgCl <sub>2</sub>	1	32.7	1400	50	4.50	0.89
	2	32.2	1400	50	4.50	3.50
	3	33.1	1400	50	4.50	12.8

For the 2M CO<sub>2</sub> concentration profiles for all the brines tested, depicted in Figure 5, similar trend was observed with regards to breakthrough times of the injected CO<sub>2</sub> as the previous 1M test. KCl had the earliest breakthrough of CO<sub>2</sub> and NaCl, CaCl<sub>2</sub>, and MgCl<sub>2</sub> had almost the same breakthrough times and their  $K_L$  values were very close. NaCl exhibited steeper concentration profile, indicating instantaneous mixing and shorter displacement front of the displacement process and thus, lower  $K_L$  compared to the other two brines (CaCl<sub>2</sub> and MgCl<sub>2</sub>) whose breakthrough times were almost the same. Again, brine concentration plays a very important role in brine distribution within the core sample with KCl brine plugging up the pore spaces and exhibiting higher  $K_L$ . This leaves no room for the interaction between the fluids within the pore spaces and, generally, earlier breakthrough times are seen in all the brine scenarios compared to the previous test of 1M ionic strength solutions.

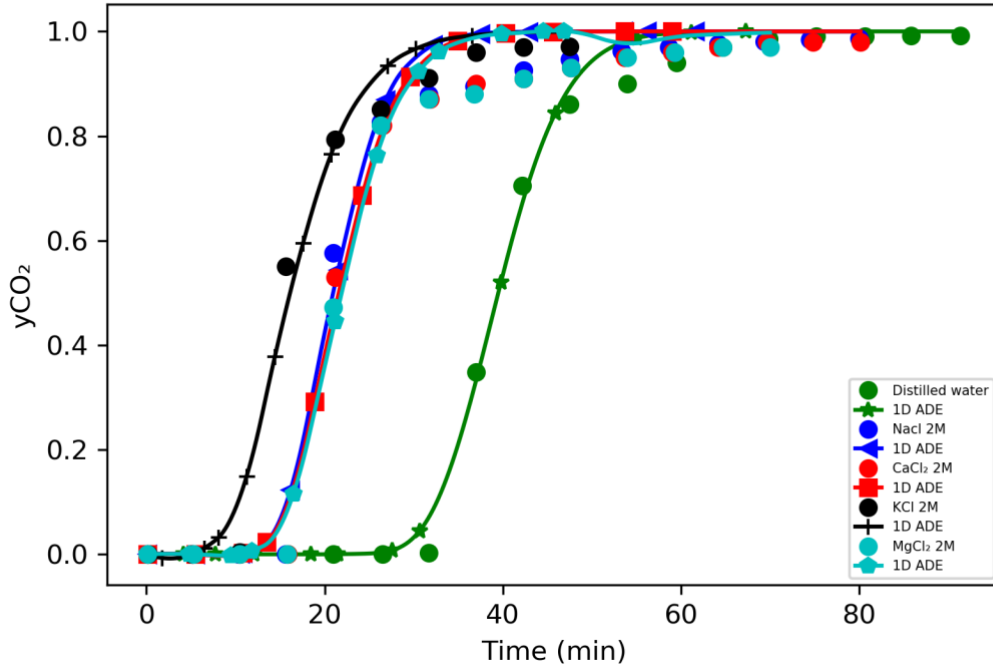


Figure 5 CO<sub>2</sub> Concentration profile at 2M ionic strength for different salt types

It goes without saying that as concentration of the brines increases, the breakthrough time for the injected CO<sub>2</sub> shortens. This is presented in Figure 6 where all the brines at 3M exhibited higher concentrations (see Figure 7). Meagre fits were observed in all the flooding scenarios, and these are as a result of the capillary entry and exit effects in short core samples during the core flooding experiments as noted by Hughes et al. (2012). However, it does not take away the validity of the results obtained, given the assumptions adopted in the 1A ADE and the fitting parameters variation during the regression. This phenomenon was also reported by Liu et al. (2015) where the fit curves were not very good especially at the later end of the concentration profile after breakthrough. And they attributed this to entry and exit effects where CH<sub>4</sub> will accumulate at the corners of the core plug and small amounts will gradually be entering the CO<sub>2</sub> flow stream exiting the core sample. The analysis in the GC of the effluent will pick up these trace amounts of the CH<sub>4</sub> and thus, CO<sub>2</sub> concentration will be lower than the that of analytical solution.

In all the brine scenarios at 3M ionic strength, there was almost immediate breakthrough within 5 minutes from the start of the CO<sub>2</sub> injection. Dispersion became substantial as seen in Table 3 where the highest  $K_L$ , exhibited by MgCl<sub>2</sub> brine, is about 6 times the magnitude of that of distilled water. Divalent brine solutions appeared to have the highest  $K_L$  and invariably the mixing of the injected CO<sub>2</sub> and nascent CH<sub>4</sub>. KCl in the monovalent category of brines exhibited the higher dispersion compared to the NaCl, largely because of the highest concentration required to prepare a brine of 3M ionic strength. This drastic shift from moderate  $K_L$  for divalent brines to high values can be attributed to salting out effects. Salting out effect is defined as the relative reduction of CO<sub>2</sub> solubility in aqueous solutions containing salts compared to CO<sub>2</sub> solubility in pore water (Messabeb et al., 2017). And divalent salts lead to

more salting out than monovalent salts. This alters the petrophysical property of the rock and affects the CO<sub>2</sub> injectivity. This increases the turbulence of the flow processes and exacerbates the mixing between the injected CO<sub>2</sub> and the displaced CH<sub>4</sub>. Furthermore, the CH<sub>4</sub> trapping phenomenon which affects the fit of the analytical solution to the experimental profile is most prevalent in this run. This is most evident in the 3M runs because of the trapping of the CH<sub>4</sub> within the corners of pore matrix by the higher concentration brines and the CO<sub>2</sub> longitudinal flow dynamics. MgCl<sub>2</sub> presented the most pronounced phenomenon because the salting out effect did little to seal off the pores where CH<sub>4</sub> was trapped and continued to allow some volumes of CH<sub>4</sub> to “leak” into the CO<sub>2</sub> flow stream. Dispersion was highest in the MgCl<sub>2</sub> experiment in the 3M run scenario as a result. KCl and CaCl<sub>2</sub> exhibited similar traits where they both plug-off the CH<sub>4</sub> traps at the corner of the core sample and CH<sub>4</sub> “leaks” into the CO<sub>2</sub> flow streams were but minimal. These will be accompanied by poor sweep efficiencies and lower CH<sub>4</sub> recoveries, as will be discussed later. Dispersion in both cases will also be lower than the MgCl<sub>2</sub> case.

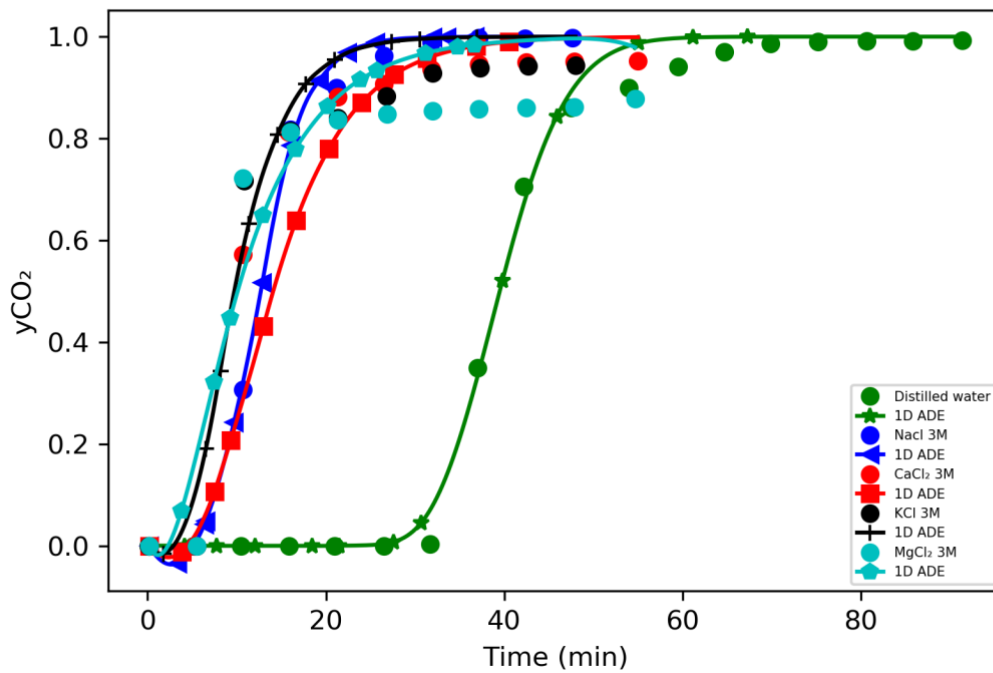


Figure 6 CO<sub>2</sub> Concentration profile at 3M ionic strength

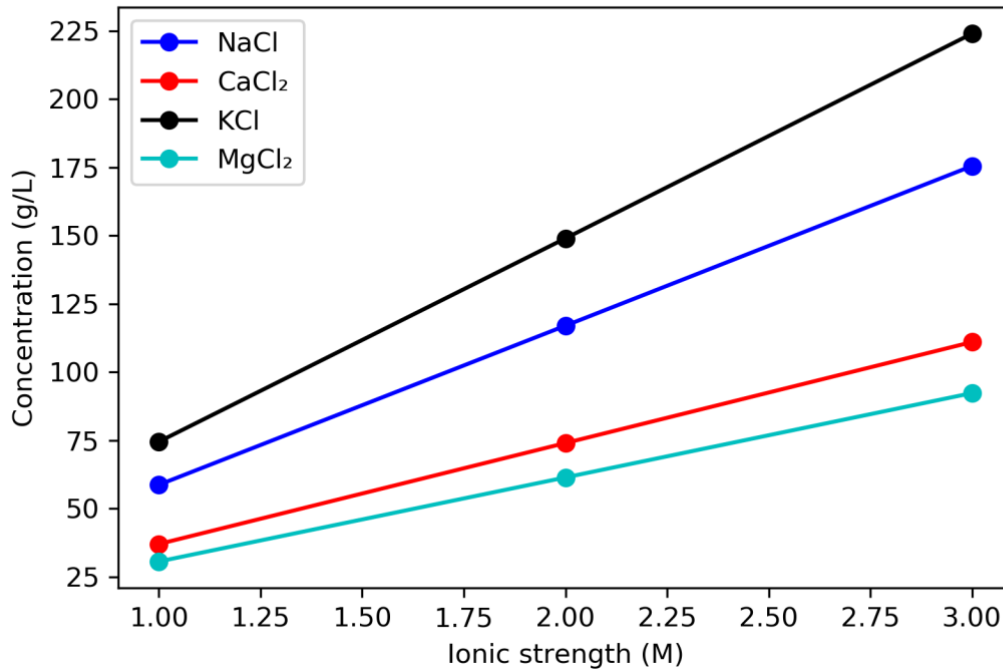


Figure 7 Brine concentrations vs ionic strengths for different salt types

### 3.2 Effects of salting out and drying out effects on dispersion coefficient

Precipitation of the salts within the core sample through salting out and drying out effects are most noticeable at higher concentrations. One of the mechanisms of these phenomena is evaporation of the brine into the stream of CO<sub>2</sub> injected (Pruess and Müller, 2009). As the CO<sub>2</sub> solubility in divalent salts decreases with increase in concentration, salting out effects become dominant and thus, the  $K_L$  increases as the flow paths of the injected CO<sub>2</sub> within the pore spaces are further constricted due to salt precipitation. A characteristic determinant of these flow restriction can be identified by observing the flow behaviour of the injected CO<sub>2</sub> as it displaces the CH<sub>4</sub>. The best way to evaluate the flow behaviour is through the differential pressure (dP) fluctuation during the core flooding process.

Figure 8 shows the dP vs time plot which depicts the flow behaviour of supercritical CO<sub>2</sub> in 1M ionic strength flooding scenario. An analogy can be made between the flow behaviour and the breakthrough times of each salt type flooding experiment. And as depicted, the flow behaviour adopted a normal displacement trend where there was generally a steady dP after CO<sub>2</sub> breakthrough. The peaks in the graphs signify the breakthrough of CO<sub>2</sub>. The highest permeability of CO<sub>2</sub> to the core sample was evident in the distilled water run which showed lowest dP profile after the breakthrough. It was earlier explained that increase in interstitial velocity was responsible for the relatively high  $K_L$ . It invariably means that as the superficial velocity increases, ultimately an increase in the flowrate ensues. Hence the direct relationship between flowrate and Darcy permeability. Lowest permeability after the breakthrough was seen in the KCl run (highest dP line after CO<sub>2</sub> breakthrough) and that can be used to explain

the restrictive flow of CO<sub>2</sub> as it passed through the core sample. The plugging of the pore spaces by the KCl at that ionic strength due to its high concentration brought about this consequence. Above all, at this ionic strength, the scale of the dP was relatively low.

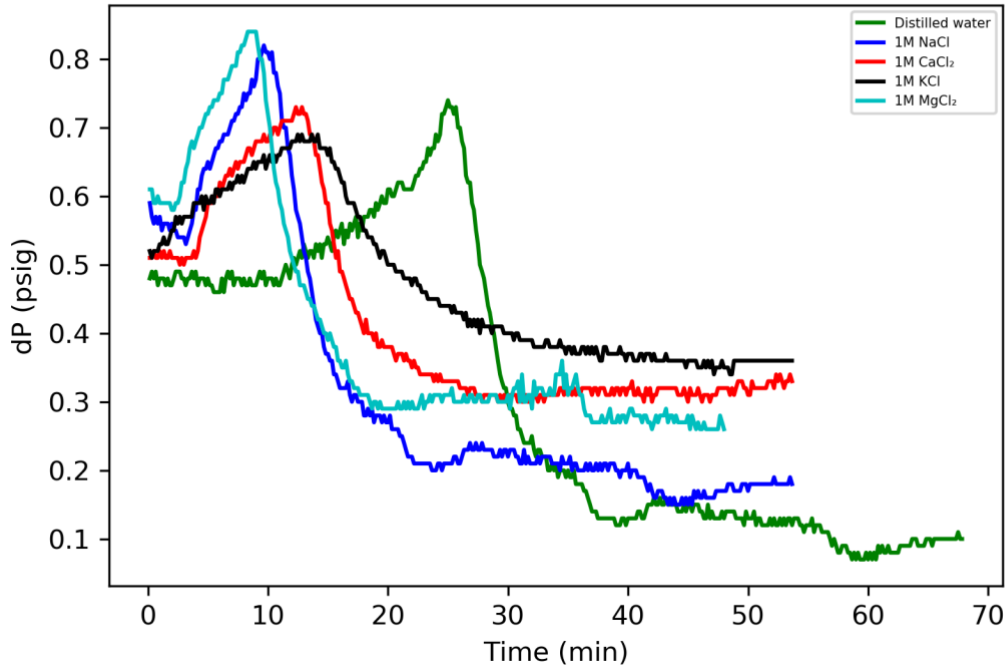


Figure 8 dP vs time schematics for flow behaviour of different brines at 1M ionic strength

For the 2M ionic strength, shown in Figure 9, the trend took a different turn, in that the scale and magnitude of the dP were higher than the 1M run. Interestingly, the divalent brines showed a peculiar behaviour after CO<sub>2</sub> breakthrough. Under ideal conditions, the dP should become steady within a slight dP range after breakthrough. However, there was a steady rise in dP for MgCl<sub>2</sub> and CaCl<sub>2</sub> brines, presenting a restrictive flow where permeability impairment was becoming evident. The monovalent brines, NaCl and KCl, showed no evidence of salting out effect at this ionic strength. Consequently, KCl still maintained the highest dP meaning that the resistance to flow of CO<sub>2</sub> within the core sample was higher than the other brine tests. Looking at Figure 7, at each ionic strength stage, the concentration of KCl far exceeded those of the other brines. Therefore, it is expected that the restrictive flow in KCl test be more pronounced than the other brines in all tests. Furthermore, the concentrations of the monovalent salts were higher than the divalent salts, but as aforementioned, salting out effect in divalent salts has more efficacy than in the monovalent salts.

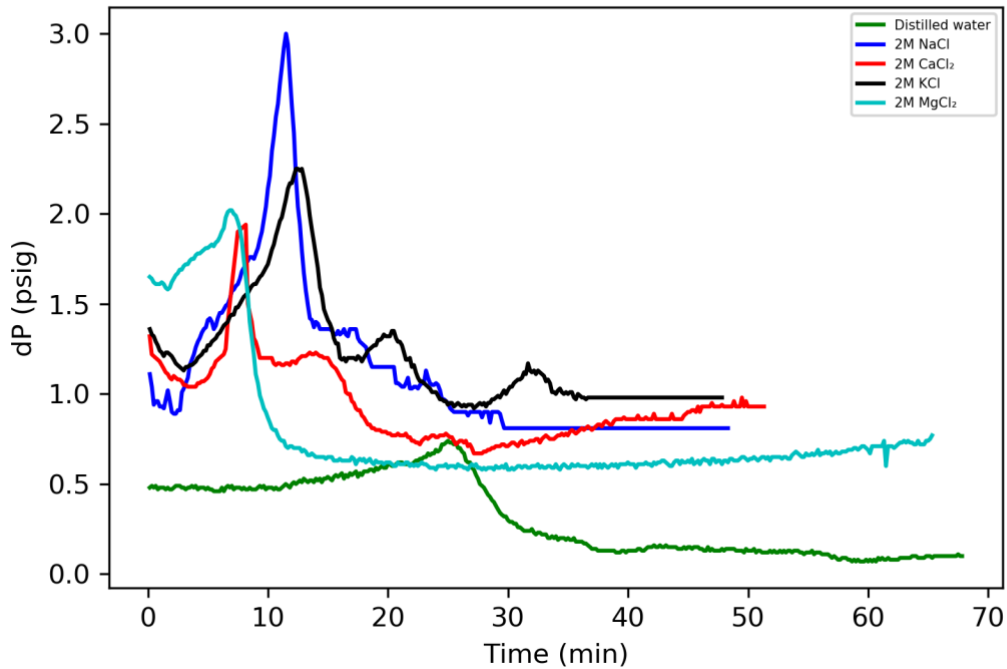


Figure 9 dP vs time schematics for flow behaviour of different brines at 2M ionic strength

Figure 10 shows typically the highest dP magnitude in all the runs so far. Here, the salting out effect, characterised by a steady increase in the dP after CO<sub>2</sub> breakthrough, was very pronounced in the divalent salts. With CaCl<sub>2</sub> showing the noticeable increase in dP over time compared to the other divalent brine, MgCl<sub>2</sub>. This is in line with the findings of (Messabeb et al., 2017) who reported that CaCl<sub>2</sub> had more susceptibility to salting out effect than MgCl<sub>2</sub> at different operating conditions but CO<sub>2</sub> solubility in both aqueous solution was similar. This is true as the flow behaviour of the divalent brines in all test conditions followed similar patterns. These flow behaviour patterns fit perfectly with the concentration profiles obtained from the previous section. The  $K_L$  obtained for all the tests can be justified with the flow behaviour of the supercritical CO<sub>2</sub> during the displacement process. Another facet/approach to this evaluation is the CH<sub>4</sub> recovery during the process in all the test brines. This will further highlight the influence of these brine types on the overall EGR process.

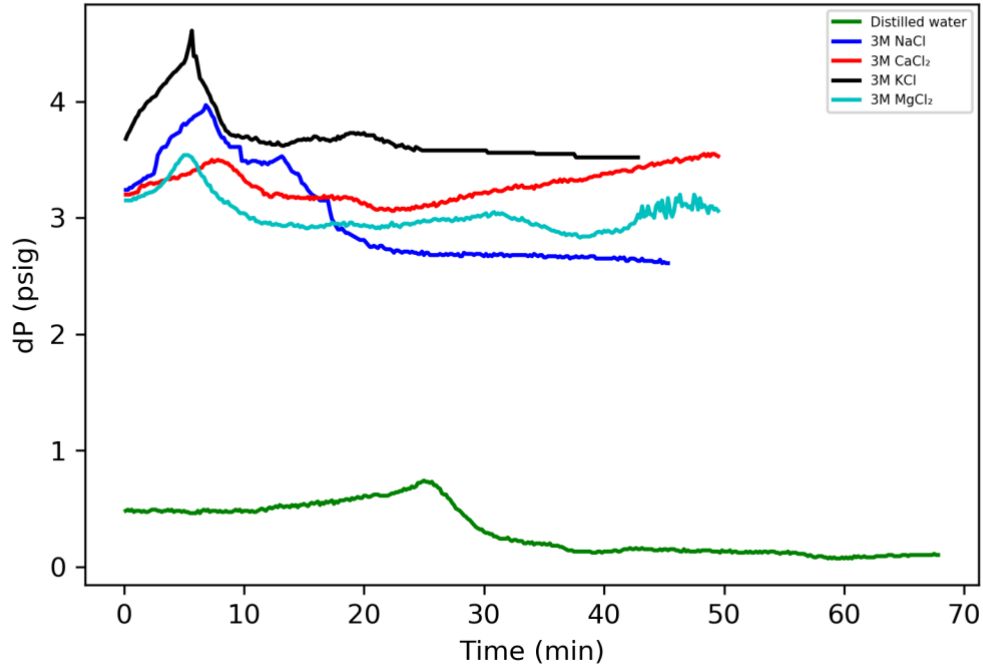


Figure 10 dP vs time schematics for flow behaviour of different brines at 3M ionic strength

### 3.3 Influence of brine type on CH<sub>4</sub> production performance

One of the reasons for the choice of natural gas reservoirs as potential sequestration sites for CO<sub>2</sub> is the CH<sub>4</sub> recovery. Here, an evaluation of the recovery factor was carried out from the analysis of the effluents from the core holder using the GC. The original gas in place (OGIP) was evaluated using the Eq. (3) as per our previous work (Abba et al., 2018b):

$$OGIP = \frac{V_b \phi (1 - S_{wi})}{B_g} \quad (3)$$

Where  $V_b$  is the bulk volume of the core sample (cm<sup>3</sup>),  $\phi$  is core sample porosity,  $S_{wi}$  is initial water saturation, and  $B_g$  is gas formation volume factor (cm<sup>3</sup>/scm<sup>3</sup>). This was used to evaluate the OGIP to obtain the recovery factors for each experimental run and condition.

Figure 11 is a depiction of the CH<sub>4</sub> recovery factors and volumetric sweep efficiencies at 1M ionic strength expressed in terms of pore volumes of CO<sub>2</sub> injected. Distilled water presented the best recovery efficiency owing to the solubility of CO<sub>2</sub> in distilled water where CH<sub>4</sub> production plateaued at about 90% of OGIP. This indicated that most of the CH<sub>4</sub> had been recovered. NaCl presented better CH<sub>4</sub> recovery than KCl and a statement can be made that monovalent brines, at 1M ionic strength, presented better CH<sub>4</sub> recovery compared to the divalent counterparts with MgCl<sub>2</sub> having the least recovery. Permeability of CO<sub>2</sub> to the core sample was better for NaCl and distilled water in this flooding scenario (Figure 8). That would explain the better recovery from these runs as the restrictive flow was not dominant and the CH<sub>4</sub> was not trapped wholly by the denser brine within the pore spaces by capillary pressure.

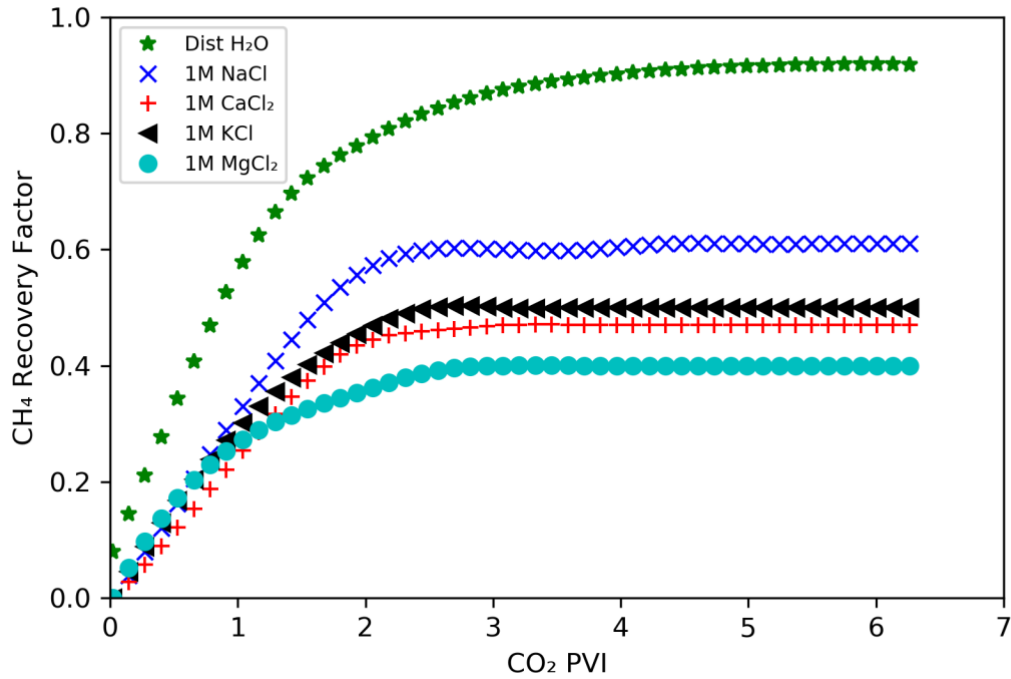


Figure 11 CH<sub>4</sub> recovery for 1M flow scenario

Invariably, the dynamics changed when the ionic strength of the brines was increased to 2M. In Figure 12, the divalent brines presented better recovery than the monovalent counterparts. This was the stage where the drying out effect took precedence and became obvious. The flow of CO<sub>2</sub> through the core sample promoted the evaporation of the moisture content in the formation brines and CH<sub>4</sub> that was dissolved in the brine during and after the drainage process came out of the solution. The concentration of the formation brines increased as a result of the evaporation. CH<sub>4</sub> solubility in brine is significantly lower than that of CO<sub>2</sub> especially in ternary systems (Qin et al., 2008). So, any offset in the equilibrium established before the injection of the CO<sub>2</sub> will eventually lead to CH<sub>4</sub> coming out of the solution. Thus, increase in CH<sub>4</sub> produced during EGR scenarios where salting out effect is pronounced will be expected. The CO<sub>2</sub> permeability in the MgCl<sub>2</sub> scenario was the highest based on the dP trend after breakthrough and it shows in the recovery efficiency schematics. Furthermore,  $K_L$  was lower in MgCl<sub>2</sub> compared to CaCl<sub>2</sub> which performed better in terms CH<sub>4</sub> recovery. Least recovery was KCl with a correspondingly highest  $K_L$  in the 2M ionic strength experimental run.

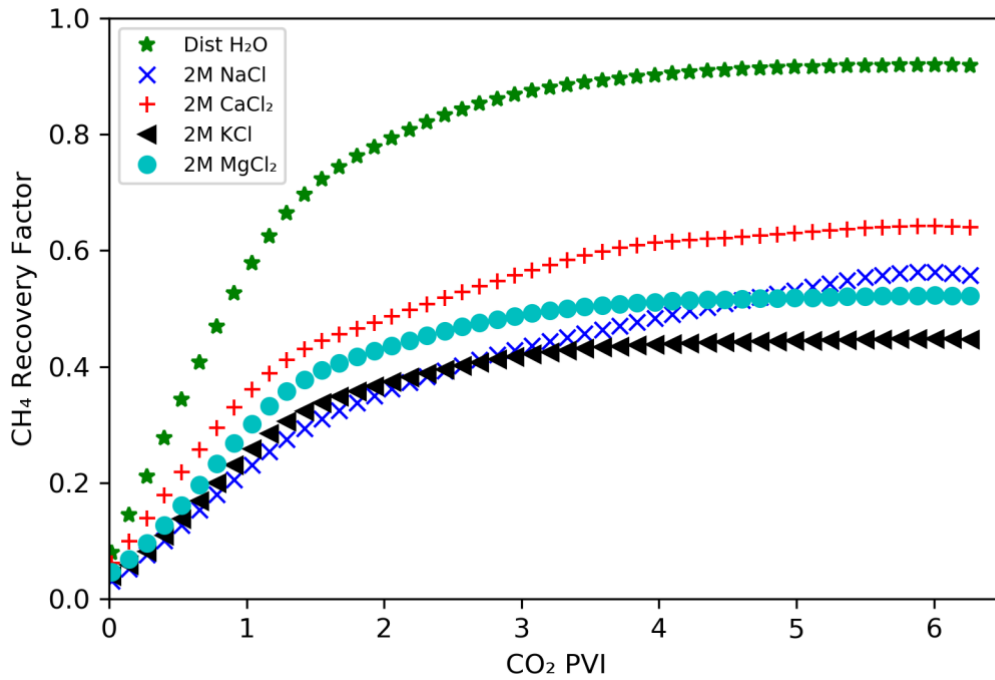


Figure 12 CH<sub>4</sub> recovery for 2M flow scenario

With the increasing ionic strength and corresponding concentration, the trend of 3M run, shown in Figure 13, depicted the worse performance in all the brine types. MgCl<sub>2</sub> still maintained the better performance for reasons mentioned earlier; salting out effect. CaCl<sub>2</sub> surprisingly did not hold up to the trend of salting out associated with better CH<sub>4</sub> recovery. At that concentration, drying out effects were more prominent in CaCl<sub>2</sub> than MgCl<sub>2</sub> as seen in Figure 10. However, the drastic plugging of the flow paths in the core sample by the extreme salting out effect of CaCl<sub>2</sub> sealed off some of the CH<sub>4</sub> and trapped it within the matrix and thus, recovery was not substantial. CH<sub>4</sub> production performance of the monovalent brines – NaCl and KCl; remained almost the same as the previous case; 2M. But NaCl had better volumetric sweep in this case compared to the KCl case.

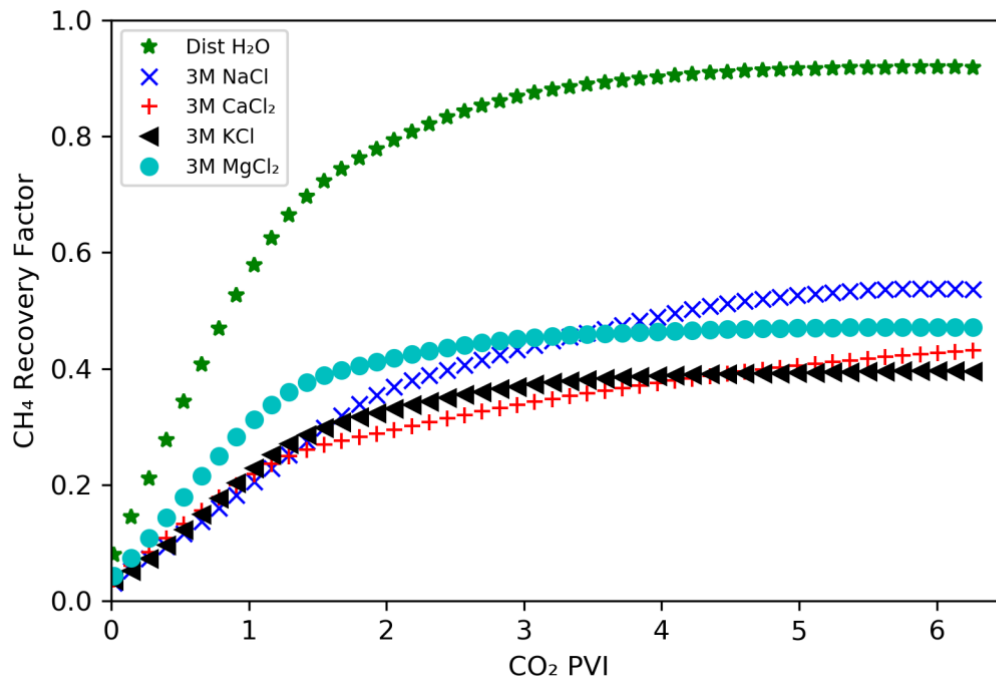


Figure 13 CH<sub>4</sub> recovery for 3M flow scenario

From all the analyses and evaluations, it can be stated that the formation brine ionic strength has strong influence on the mixing of the injected CO<sub>2</sub> and the nascent CH<sub>4</sub> during EGR processes. In our previous work (Abba et al., 2018b), we postulated that as the density/salinity of the connate water increases, the CO<sub>2</sub> dispersion coefficient decreases. This, however, was proposed on the premise of salinities of up to 10 wt.% NaCl. Figure 14 shows the relationship between  $K_L$  and ionic strengths of different salts types. The difference in the current NaCl run and the one obtained by Abba et. al., (2018b) was as result of using different core samples with different petrophysical properties. However, there is an agreement in the trend of  $K_L$  decreasing with increasing salinities up to 10 wt.%. Then the  $K_L$  increases rather sharply and drastically, especially for MgCl<sub>2</sub> and CaCl<sub>2</sub>, as the salinity increases. As expected, the divalent salts demonstrated similar trends owing to their salting out similarities as earlier stated. The monovalent salts, NaCl and KCl, on the other hand presented a dissimilarity in terms of performance but the profiles of the  $K_L$  vs ionic strength/salinity appeared the same. The relationship between  $K_L$  and formation water salinity can be described by a hyperbolic-like curve. Therefore, this gives a good indication of the best ranges of salinities to fully exploit natural gas reservoirs in all their potential for EGR. Lowest contamination of the recovered CH<sub>4</sub> can be postulated to be expected in natural gas reservoirs with connate water salinities between 5-15 wt.% during EGR by CO<sub>2</sub> injection. More importantly, the composition of the formation water and the presence of divalent salts at higher concentrations of the brine formulation will certainly play a major role in the recovery efficiency of the CH<sub>4</sub>.

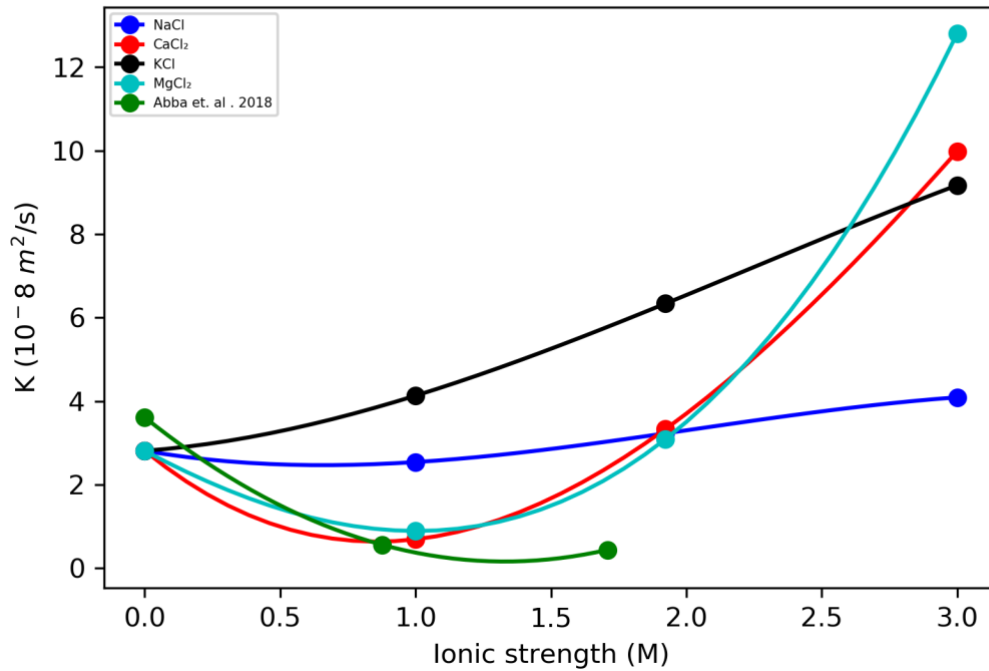


Figure 14 Variation of  $K_L$  with ionic strength for different brine scenarios

Furthermore,  $\text{CO}_2$  storage will be affected by the brine composition, given the mutual solubilities of  $\text{CH}_4$  and  $\text{CO}_2$  in the formation water at different conditions in a ternary system. This study will be vital in the design of any  $\text{CO}_2$  sequestration process for simulation studies and eventual field scale applications of EGR.

## 4 Conclusion and future work

The evaluation of the effects of brine type and concentration on the dispersion coefficient was carried out using a methodical core flooding process. The study follows the investigation of  $\text{CO}_2$  dispersion coefficient in different brine with different ionic strengths, the flow behaviour of supercritical  $\text{CO}_2$ , and  $\text{CH}_4$  production performance during EGR. From these analyses, the following conclusions can be drawn:

- At lower ionic strength of 1M, lowest  $\text{CO}_2$  dispersion coefficients were realised for  $\text{MgCl}_2$  and  $\text{CaCl}_2$  brines with  $0.89 \times 10^{-8} \text{ m}^2/\text{s}$  and  $0.69 \times 10^{-8} \text{ m}^2/\text{s}$  respectively. On the contrary, NaCl and KCl brines exhibited higher dispersion coefficients by a factor of 4 – 6 respectively.
- Salting out effect was responsible for the higher dispersion coefficients observed in  $\text{MgCl}_2$  and  $\text{CaCl}_2$  ( $12.8 \times 10^{-8} \text{ m}^2/\text{s}$  and  $9.98 \times 10^{-8} \text{ m}^2/\text{s}$  respectively) because of their susceptibility to drying out at higher concentrations. Thus, enabling a more turbulent  $\text{CO}_2$  flow (by increasing the interstitial velocity) within the reduced pore spaces which intensifies mixing between  $\text{CO}_2$  and  $\text{CH}_4$ .

- As the brine moisture evaporates due to the drying and salting out effects during CO<sub>2</sub> injection, an increase in the recovered CH<sub>4</sub> was realised from the divalent brines at ionic strength of 2M with CH<sub>4</sub> coming out of solution.
- CO<sub>2</sub> storage can be promoted by the solubility of CO<sub>2</sub> in the formation brine. With NaCl being the dominant salt type in formation water, large volumes of CO<sub>2</sub> can safely be sequestered in natural gas reservoirs. This indicates the potential to increase their storage capacities by including solubility trapping as additional trapping mechanism in conjunction with structural trapping. But its worthy of note, that the presence of divalent salts may also affect the storability of natural gas reservoirs, especially at higher concentrations.
- Lowest contamination of the recovered natural gas is postulated to be expected in natural gas reservoirs with formation water salinities between 5-15 wt.% during EGR by CO<sub>2</sub> injection and sequestration.
- Dispersion coefficient is also dependent on the ionic strength/salinity and type of the formation brine during EGR. A hyperbolic relationship exists between the two properties, where  $K_L$  decreases from 0 to 1M, and then increases drastically from >1M ionic strength. This sharp increasing trend was more prominent in the divalent brines than in the monovalent brines partly, because of the dynamics of properties of the brines tested.

The study was based on the ionic strengths of different brine types in consolidated porous media. It investigated the interplay between the fluids in the ternary systems in terms of production performance, dispersion coefficient variation, CO<sub>2</sub> storability, and flow behaviour for EGR in natural gas reservoirs. This can be extended to CO<sub>2</sub> injection in deep saline for CO<sub>2</sub> sequestration where more light can be shed on the injectivity of CO<sub>2</sub> during storage. Furthermore, future will look at the mixture of these salts in varying proportion to evaluate the limiting combination to the effectiveness of EGR by CO<sub>2</sub> injection and sequestration in consolidated porous media.

### **Declaration of Competing Interest**

The author declares that they have no known competing financial interests or personal relationships that could have appeared to influence the work reported in this study.

### **Acknowledgment**

The author would like to acknowledge the Petroleum and Spray Research Group (PTSRG) for consultation and support.

### **References**

- Abba, M.K., 2018. Role of Connate Water Salinity in Gas Dispersion during Enhanced Gas Recovery by Carbon dioxide Injection and Sequestration Muhammad. Univ. Salford. <https://doi.org/10.1017/CBO9781107415324.004>
- Abba, Muhammad Kabir, Abbas, A.J., Al-Othaibi, A., Nasr, G.G., 2018a. Enhanced Gas

- Recovery by CO<sub>2</sub> Injection and Sequestration: Effects of Temperature, Vertical and Horizontal Orientations on Dispersion Coefficient, in: SPE Abu Dhabi International Petroleum Exhibition & Conference.
- Abba, M.K., Abbas, A.J., Nasr, G.G., 2017. Enhanced gas recovery by CO<sub>2</sub> injection and sequestration: Effect of connate water salinity on displacement efficiency, in: Society of Petroleum Engineers - SPE Abu Dhabi International Petroleum Exhibition and Conference 2017.
- Abba, M.K., Abbas, A.J., Nasr, G.G., Al-Otaibi, A., Burby, M., Saidu, B., Suleiman, S.M., 2019a. Solubility trapping as a potential secondary mechanism for CO<sub>2</sub> sequestration during enhanced gas recovery by CO<sub>2</sub> injection in conventional natural gas reservoirs: An experimental approach. *J. Nat. Gas Sci. Eng.* 71, 103002. <https://doi.org/10.1016/j.jngse.2019.103002>
- Abba, M.K., Al-Otaibi, A., Abbas, A.J., Nasr, G.G., 2019b. Influence of Permeability and Injection Orientation Variations on Dispersion Coefficient during Enhanced Gas Recovery by CO<sub>2</sub> Injection. *Energies* 12, 2328. <https://doi.org/https://doi.org/10.3390/en12122328>
- Abba, Muhammad Kabir, Al-Othaibi, A., Abbas, A.J., Nasr, G.G., Mukhtar, A., 2018b. Experimental investigation on the impact of connate water salinity on dispersion coefficient in consolidated rocks cores during Enhanced Gas Recovery by CO<sub>2</sub> injection. *J. Nat. Gas Sci. Eng.* <https://doi.org/10.1016/j.jngse.2018.10.007>
- Abba, M.K., Al-Othaibi, A., Abbas, A.J., Nasr, G.G., Mukhtar, A., 2018. Experimental investigation on the impact of connate water salinity on dispersion coefficient in consolidated rocks cores during Enhanced Gas Recovery by CO<sub>2</sub> injection. *J. Nat. Gas Sci. Eng.* 60. <https://doi.org/10.1016/j.jngse.2018.10.007>
- Adepoju, O.O., Lake, L.W., Johns, R.T., 2013. Investigation of Anisotropic Mixing in Miscible Displacements. *SPE Reserv. Eval. Eng.* 16, 85–96.
- Ahmad, N., Wörman, A., Sanchez-Vila, X., Jarsjö, J., Bottacin-Busolin, A., Hellevang, H., 2016. Injection of CO<sub>2</sub>-saturated brine in geological reservoir: A way to enhanced storage safety. *Int. J. Greenh. Gas Control* 54, 129–144. <https://doi.org/10.1016/j.ijggc.2016.08.028>
- Al-Abri, A., Sidiq, H., Amin, R., 2012. Mobility ratio, relative permeability and sweep efficiency of supercritical CO<sub>2</sub> and methane injection to enhance natural gas and condensate recovery: Coreflooding experimentation. *J. Nat. Gas Sci. Eng.* 9, 166–171. <https://doi.org/10.1016/j.jngse.2012.05.011>
- Bennaceur, K., 2013. CO<sub>2</sub> Capture and Sequestration. *Futur. Energy Improv. Sustain. Clean Options our Planet* 583–611. <https://doi.org/10.1016/B978-0-08-099424-6.00026-0>
- Benson, S.M., Cole, D.R., 2008. CO<sub>2</sub> sequestration in deep sedimentary formations. *Elements* 4, 325–331. <https://doi.org/10.2113/gselements.4.5.325>
- Ding, S., Xi, Y., Jiang, H., Liu, G., 2018. CO<sub>2</sub> storage capacity estimation in oil reservoirs by solubility and mineral trapping. *Appl. Geochemistry* 89, 121–128. <https://doi.org/10.1016/j.apgeochem.2017.12.002>
- Ekwere, P.J., 2007. Petrophysics.
- Feather, B., Archer, R.A., 2010. Enhanced Natural Gas Recovery by Carbon Dioxide Injection for Storage Purposes.
- Honari, A., Bijeljic, B., Johns, M.L., May, E.F., 2015. Enhanced gas recovery with {CO<sub>2</sub>} sequestration: The effect of medium heterogeneity on the dispersion of supercritical CO<sub>2</sub>–CH<sub>4</sub>. *Int. J. Greenh. Gas Control* 39, 39–50. <https://doi.org/http://dx.doi.org/10.1016/j.ijggc.2015.04.014>
- Honari, A., Hughes, T.J., Fridjonsson, E.O., Johns, M.L., May, E.F., 2013. Dispersion of supercritical CO<sub>2</sub> and CH<sub>4</sub> in consolidated porous media for enhanced gas recovery

- simulations. *Int. J. Greenh. Gas Control* 19, 234–242.  
<https://doi.org/10.1016/j.ijggc.2013.08.016>
- Honari, A., Zecca, M., Vogt, S.J., Iglauer, S., Bijeljic, B., Johns, M.L., May, E.F., 2016. The impact of residual water on CH<sub>4</sub>-CO<sub>2</sub> dispersion in consolidated rock cores. *Int. J. Greenh. Gas Control* 50, 100–111. <https://doi.org/10.1016/j.ijggc.2016.04.004>
- Hughes, T.J., Honari, A., Graham, B.F., Chauhan, A.S., Johns, M.L., May, E.F., 2012. CO<sub>2</sub> sequestration for enhanced gas recovery: New measurements of supercritical CO<sub>2</sub>-CH<sub>4</sub> dispersion in porous media and a review of recent research. *Int. J. Greenh. Gas Control* 9, 457–468. <https://doi.org/10.1016/j.ijggc.2012.05.011>
- Kalantari-Dahaghi, A., Mohaghegh, S., He, Q., 2013. CO<sub>2</sub>-Driven Enhanced Gas Recovery and Storage in Depleted Shale Reservoir- A Numerical Simulation Study. *Carbon Manag. Technol. Conf. Proc.* c.
- Kalra, S., Wu, X., 2014. CO<sub>2</sub> injection for Enhanced Gas Recovery. *SPE West. North Am. Rocky Mt. ...* 16–18.
- Kumar, S., Foroozesh, J., Edlmann, K., Rezk, M.G., Lim, C.Y., 2020. A comprehensive review of value-added CO<sub>2</sub> sequestration in subsurface saline aquifers. *J. Nat. Gas Sci. Eng.* 81, 103437. <https://doi.org/10.1016/j.jngse.2020.103437>
- Liu, S., Song, Y., Zhao, C., Zhang, Y., Lv, P., Jiang, L., Liu, Y., Zhao, Y., 2018. The horizontal dispersion properties of CO<sub>2</sub>-CH<sub>4</sub> in sand packs with CO<sub>2</sub> displacing the simulated natural gas. *J. Nat. Gas Sci. Eng.* 50, 293–300.  
<https://doi.org/10.1016/j.jngse.2017.12.019>
- Liu, S., Zhang, Y., Xing, W., Jian, W., Liu, Z., Li, T., Song, Y., 2015. Laboratory experiment of CO<sub>2</sub>-CH<sub>4</sub> displacement and dispersion in sandpacks in enhanced gas recovery. *J. Nat. Gas Sci. Eng.* 26, 1585–1594. <https://doi.org/10.1016/j.jngse.2015.04.021>
- Liu, S., Zhang, Y., Zhao, J., Jiang, L., Song, Y., 2020. Dispersion characteristics of CO<sub>2</sub> enhanced gas recovery over a wide range of temperature and pressure. *J. Nat. Gas Sci. Eng.* 73, 103056. <https://doi.org/10.1016/j.jngse.2019.103056>
- Messabeh, H., Contamine, F., Cézac, P., Serin, J.P., Pouget, C., Gaucher, E.C., 2017. Experimental Measurement of CO<sub>2</sub> Solubility in Aqueous CaCl<sub>2</sub> Solution at Temperature from 323.15 to 423.15 K and Pressure up to 20 MPa Using the Conductometric Titration. *J. Chem. Eng. Data* 62, 4228–4234.  
<https://doi.org/10.1021/acs.jced.7b00591>
- Newberg, M., Foh, S., 1988. Measurement of Longitudinal Dispersion Coefficients for Gas Flowing Through Porous Media. *SPE* 5–9.
- Nogueira, M., Mamora, D.D., 2005. Effect of Flue-Gas Impurities on the Process of Injection and Storage of CO<sub>2</sub> in Depleted Gas Reservoirs. *J. Energy Resour. Technol.* 130, 013301. <https://doi.org/10.1115/1.2825174>
- Oldenburg, C.M., 2003. Carbon Sequestration in natural Gas Reservoirs: Enhanced Gas Recovery and natural Gas Storage. *TOUGH Symp.* 2003 1–8.
- Oldenburg, C.M., Benson, S.M., 2002. CO<sub>2</sub> Injection for Enhanced Gas Production and Carbon Sequestration. *SPE Int. Pet. Conf. Exhib. Mex.* <https://doi.org/10.2118/74367-MS>
- Perkins, T., Johnston, O., 1963. A Review of Diffusion and Dispersion in Porous Media. *Soc. Pet. Eng. J.* 3, 70–84. <https://doi.org/10.2118/480-PA>
- Pruess, K., Müller, N., 2009. Formation dry-out from CO<sub>2</sub> injection into saline aquifers: 1. effects of solids precipitation and their mitigation. *Water Resour. Res.* 45, 1–11.  
<https://doi.org/10.1029/2008WR007101>
- Qin, J., Rosenbauer, R.J., Duan, Z., 2008. Experimental measurements of vapor-liquid equilibria of the H<sub>2</sub>O + CO<sub>2</sub> + CH<sub>4</sub> ternary system. *J. Chem. Eng. Data* 53, 1246–1249.  
<https://doi.org/10.1021/jc700473e>

- Raza, A., Gholami, R., Rezaee, R., Bing, C.H., Nagarajan, R., Hamid, M.A., 2017. Preliminary assessment of CO<sub>2</sub> injectivity in carbonate storage sites. *Petroleum* 3, 144–154. <https://doi.org/10.1016/j.petlm.2016.11.008>
- Rochelle, C. a., Moore, Y. a., 2002. The solubility of supercritical CO<sub>2</sub> into pure water and synthetic Utsira porewater, Indman.Sintef.No.
- Sidiq, H., Amin, R., 2009. Mathematical model for calculating the dispersion coefficient of super critical CO<sub>2</sub> from the results of laboratory experiments on enhanced gas recovery. *J. Nat. Gas Sci. Eng.* 1, 177–182. <https://doi.org/10.1016/j.jngse.2009.11.001>
- Sim, S, Turta, A.T., Singhal, A., Hawkins, B.F., 2009. Enhanced Gas Recovery: Effect of Reservoir Heterogeneity on Gas-Gas Displacement. *Candian Int. Pet. Conf.* 1–14. <https://doi.org/10.2118/2009-023>
- Sim, Sim, Turta, A.T., Singhal, A.K., Hawkins, B.F., 2009. Enhanced gas recovery: Factors affecting gas-gas displacement efficiency. *J. Can. Pet. Technol.* 48, 49–55. <https://doi.org/10.2118/09-08-49>
- Tong, D., Trusler, J.P.M., Vega-Maza, D., 2013. Solubility of CO<sub>2</sub> in aqueous solutions of CaCl<sub>2</sub> or MgCl<sub>2</sub> and in a synthetic formation brine at temperatures up to 423 K and pressures up to 40 MPa. *J. Chem. Eng. Data* 58, 2116–2124. <https://doi.org/10.1021/je400396s>
- Turta, A., Sim, S., Singhal, A.K., Hawkins, B.F., 2007. Basic Investigations on Enhanced Gas Recovery by Gas-Gas Displacement.
- Turta, A.T., Sim, S.S.K., Singhal, A., Hawkins, B.F., 2007. Basic Investigations on Enhanced Gas Recovery by Gas-Gas Displacement 2 . 2 Composition of CO<sub>2</sub> – Containing Gas Streams to be Used for EGR, in: *Canadian International Petroleum Conference*.
- U.S. EPA, 2019. Inventory of U.S. Greenhouse Gas Emissions and Sinks: 1990-2018, EPA Report 430-R-20-002. <https://doi.org/10.1017/CBO9781107415324.004>
- Zecca, M., Vogt, S.J., Honari, A., Xiao, G., Fridjonsson, E.O., May, E.F., Johns, M.L., 2017. Quantitative dependence of CH<sub>4</sub>-CO<sub>2</sub> dispersion on immobile water fraction. *AIChE J.* 63, 5159–5168. <https://doi.org/10.1002/aic.15824>
- Zhang, D., Song, J., 2013a. Mechanisms for geological carbon sequestration. *Procedia IUTAM* 10, 319–327. <https://doi.org/10.1016/j.piutam.2014.01.027>
- Zhang, D., Song, J., 2013b. Mechanisms for geological carbon sequestration. *Procedia IUTAM* 10, 319–327. <https://doi.org/10.1016/j.piutam.2014.01.027>
- Zhang, Y., Liu, S., Song, Y., Zhao, J., Tang, L., Xing, W., Jian, W., Liu, Z., Zhan, Y., 2014. Experimental investigation of CO<sub>2</sub>-CH<sub>4</sub> displacement and dispersion in sand pack for enhanced gas recovery. *Energy Procedia* 61, 393–397. <https://doi.org/10.1016/j.egypro.2014.11.1133>